Coronavirus Hot Paper

How to cite: *Angew. Chem. Int. Ed.* **2021**, *60*, 21211–21215
International Edition: doi.org/10.1002/anie.202107730
German Edition: doi.org/10.1002/ange.202107730

Discovery and Characterization of Spike N-Terminal Domain-Binding Aptamers for Rapid SARS-CoV-2 Detection

Nataly Kacherovsky[+], Lucy F. Yang[+], Ha V. Dang[+], Emmeline L. Cheng, Ian I. Cardle, Alexandra C. Walls, Matthew McCallum, Drew L. Sellers, Frank DiMaio, Stephen J. Salipante, Davide Corti, David Veesler, and Suzie H. Pun**

Abstract: *The coronavirus disease 2019 (COVID-19) pandemic has devastated families and disrupted healthcare, economies and societies across the globe. Molecular recognition agents that are specific for distinct viral proteins are critical components for rapid diagnostics and targeted therapeutics. In this work, we demonstrate the selection of novel DNA aptamers that bind to the SARS-CoV-2 spike glycoprotein with high specificity and affinity (< 80 nM). Through binding assays and high resolution cryo-EM, we demonstrate that SNAP1 (SARS-CoV-2 spike protein N-terminal domain-binding aptamer 1) binds to the S N-terminal domain. We applied SNAP1 in lateral flow assays (LFAs) and ELISAs to detect UV-inactivated SARS-CoV-2 at concentrations as low as* 5×10^5 *copies* mL^{-1}*. SNAP1 is therefore a promising molecular tool for SARS-CoV-2 diagnostics.*

Effective disease control of the COVID-19 pandemic, caused by severe acute respiratory syndrome coronavirus 2 (SARS-CoV-2)[1] includes early detection of SARS-CoV-2 infections.[2] Despite the deployment of COVID-19 vaccines,[3] SARS-CoV-2 diagnostic tools remain critical for reducing virus spread. Furthermore, advances in rapid diagnostics enable better preparation for future pandemics.[4]

COVID-19 diagnostic tests for active infections include molecular tests that detect viral RNA by nucleic acid amplification, and rapid antigen tests that detect viral proteins. While molecular tests are extremely sensitive and specific,[5] rapid antigen tests are simpler to administer, provide point-of-care results, and are less expensive than molecular tests.[6] Rapid antigen testing reduces COVID-19 prevalence by an estimated 70% compared to unmitigated growth.[7]

A major SARS-CoV-2 antigen detected by COVID-19 diagnostics is the spike (S) protein, a transmembrane glycoprotein that protrudes from the viral envelope.[8] Antibodies against SARS-CoV-2 S protein have been isolated,[9] and mRNA encoding the S protein is the basis of FDA-authorized mRNA vaccines.[10] SARS-CoV-2, a betacoronavirus, is closely related to SARS-CoV, which caused the 2002–2003 Severe Acute Respiratory Syndrome epidemic, and more distantly related to the MERS-CoV responsible for the 2012 Middle East Respiratory Syndrome outbreak, sharing ≈72% and ≈35% sequence similarity, respectively, with the S proteins of these viruses.[8b] The SARS-CoV-2 S protein is composed of three identical monomers with two distinct subunits.[11] Subunit 1 (S1) contains a receptor binding domain (RBD), which binds to human angiotensin-converting enzyme 2 (ACE2) and mediates host cell recognition, and an N-terminal domain (NTD).[8a,11a] Recently, an antigenic supersite on the NTD was found to be frequently targeted by NTD-binding antibodies,[9a] indicating that binders to this site may play a role in specific recognition of and immunity to SARS-CoV-2.

Aptamers are short nucleic acid sequences that bind target molecules. Aptamers not only achieve specific binding with affinities on par with antibodies, but also are cheaper and easier to produce.[12] Novel aptamers are discovered through a library selection method coined systematic evolution of ligands by exponential enrichment (SELEX).[13] For detection of intact SARS-CoV-2 virus, aptamers that bind to accessible surface proteins such as S are needed.

In this study, we report the discovery and optimization of DNA aptamers that bind SARS-CoV-2 S protein with high affinity and specificity. We identified the aptamers' binding epitope as the NTD of the SARS-CoV-2 S protein by biolayer interferometry (BLI) and cryogenic electron microscopy (Cryo-EM). Currently, there are reports of aptamers binding to RBD of SARS-CoV-2.[14] To our knowledge, the aptamers reported here are the first to bind the NTD of SARS-CoV-2 S. In addition, we present the first cryo-EM map of SARS-CoV-2 S in complex with a DNA aptamer. We then used SNAP1 to detect both S protein and UV-inactivated SARS-CoV-2 by lateral flow assay (LFA) and by ELISA.

[*] N. Kacherovsky,[+] L. F. Yang,[+] E. L. Cheng, I. I. Cardle, Prof. D. L. Sellers, Prof. S. H. Pun
Department of Bioengineering, University of Washington
Seattle, WA 98105 (USA)
E-mail: spun@uw.edu

H. V. Dang,[+] Dr. A. C. Walls, Dr. M. McCallum, Prof. F. DiMaio, Prof. D. Veesler
Department of Biochemistry, University of Washington
Seattle, WA 98105 (USA)
E-mail: dveesler@uw.edu

Prof. S. J. Salipante
Department of Laboratory Medicine, University of Washington
Seattle, WA 98105 (USA)

Dr. D. Corti
Humabs BioMed SA, a subsidiary of Vir Biotechnology
6500 Bellinzona (Switzerland)

[+] These authors contributed equally to this work.

Supporting information and the ORCID identification number(s) for the author(s) of this article can be found under https://doi.org/10.1002/anie.202107730. The cryoEM maps have been deposited to the electron microscopy data bank with accession numbers EMD-24678 (global reconstruction) and EMD-24679 (local refinement of the SNAP1/NTD region).

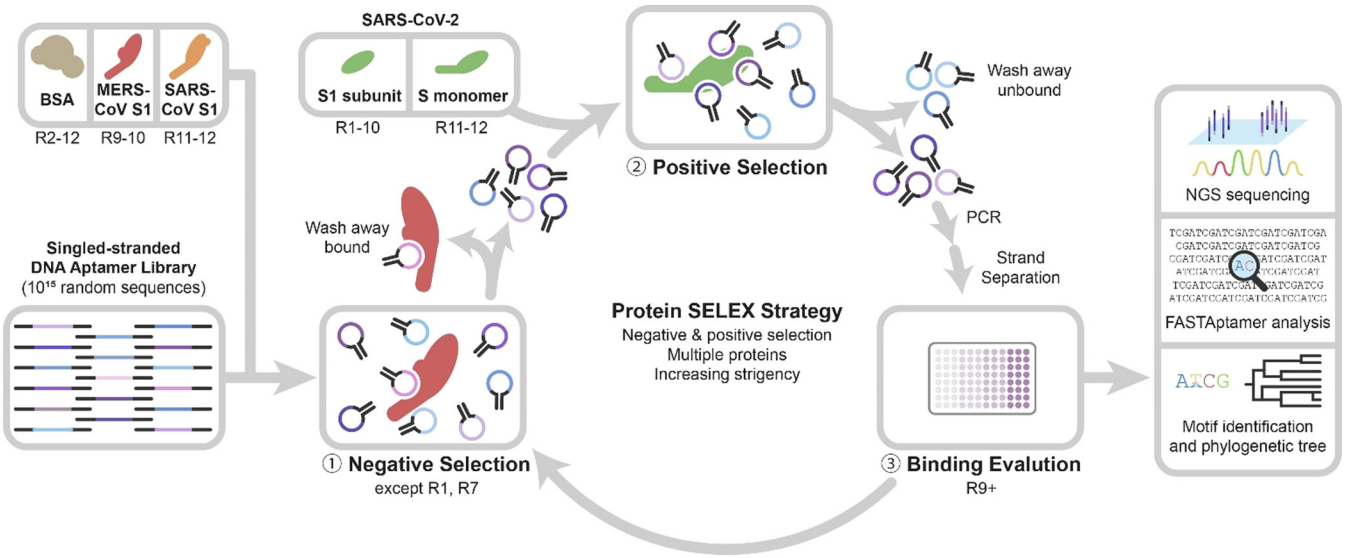

Figure 1. Schematic of protein-SELEX strategy using a DNA aptamer library. After an initial round of positive selection, subsequent rounds consisted of negative and positive selection with increasingly stringent conditions (Table S1). Negative selection included control proteins (BSA, MERS-CoV S1, or SARS-CoV S1) and protein immobilization platforms.

We designed a protein SELEX strategy using the SARS-CoV-2 S protein as the binding target (Figure 1). To minimize selection of non-specific aptamers, we alternated the protein tag (His- and Fc-tag) and corresponding partitioning platforms and increased selective pressure by adding multiple competitors including MERS-CoV S1 and SARS-CoV S1 (Table S1). Using an ELISA-like plate binding assay, we detected a 15-fold increase in aptamer binding in the round 11 aptamer pool without a further increase in binding for round 12, indicating that selection was complete (Figure S1). We sequenced the selection rounds (Table S2) and analyzed results by FASTAptamer.[15] By round 12, the library had shrunk considerably, and our top aptamer motif (motif 1) accounted for 64.3 % of all sequences (Table S3, Figure S2). A closely related motif (motif 3) was also present in two of the top 100 ranking aptamers. We characterized the aptamers containing motif 1 (later named SNAP1) and motif 3 (later named SNAP3) (Table S4). The predicted secondary structures of the aptamers SNAP1 and SNAP3 and their sequence similarities are shown in Figure S3A-B.

We demonstrated that Cy5-labeled SNAP1 and SNAP3 bind specifically to SARS-CoV-2 S1 but not SARS-CoV and MERS-CoV S1 proteins using flow cytometry binding studies (Figure S4 and S5A). No SNAP1 or SNAP3 binding was observed to a control protein (CD71), and a non-specific (NS) aptamer sequence did not show binding to S1. We further confirmed specificity using biolayer interferometry (BLI) to monitor protein association to immobilized aptamers. We observed that SNAP1 and SNAP3 bind SARS-CoV-2 S1 at <10 nM protein (Figure 2 A). In addition, SNAP1 did not bind to SARS-CoV S1 or MERS-CoV S1 even at 200 nM protein (Figure S5B). Thus, both aptamers target SARS-CoV-2 S1 with high specificity.

We investigated whether SNAP1 and SNAP3 bind the RBD by ACE2 competition studies but observed no change in binding constants between SARS-CoV-2 S1 and ACE2 in the presence of large excesses of aptamer either by BLI (Figure S6A) or flow cytometry (Figure S6B). We then used BLI to characterize binding of SNAP1 and SNAP3 to SARS-CoV-2 S1 and S1 NTD. Using aptamer-functionalized (SNAP1, SNAP3, and NS) sensors, we determined that the K_D of S1 binding to SNAP1 (39.32 ± 0.12 nM) was about 2-fold lower than that of SNAP3 (76.59 ± 0.45 nM) (Figure 2 A, Table S5). NS aptamer did not bind to SARS-CoV-2 S1 (Figure S5B). We observed similar equilibrium constants of aptamer binding to S1 NTD as that of S1 (SNAP1 $K_D = 60.35 \pm 1.61$ nM, and SNAP3 $K_D = 53.25 \pm 2.49$ nM for NTD binding) (Figure 2 A), indicating that aptamer binding is localized to the NTD on SARS-CoV-2 S1 protein. Accordingly, the aptamers were named SARS-CoV-2 Spike protein NTD-binding APtamers 1 and 3, or SNAP1 and SNAP3, respectively.

We investigated whether SNAP1 and SNAP3 bind to the same NTD site through competition studies. We observed that SNAP3 binding to S1 was reduced to about 50 % of maximum binding in the presence of equal amount of SNAP1 (Figure S7), suggesting that SNAP1 and SNAP3 bind to an overlapping epitope on NTD. We therefore used SNAP1 for Cryo-EM characterization.

We determined a Cryo-EM structure of SARS-CoV-2 S bound to SNAP1 in the presence of the S2M11 neutralizing antibody, which overcame preferential specimen orientation in vitreous ice and limited S conformational variability[9e] (Figure S8A-B). We obtained a cryo-EM map at an overall 3.3 Å resolution applying three-fold symmetry (Figure 2 B, Figure S8C). The map was best resolved at the SARS-CoV-2 S core, whereas SNAP1 showed a high degree of flexibility outside of its binding contact region with SARS-CoV-2 S (Figure S8D). SNAP1 adopted an overall double-stranded helical shape, extending outwards from the SARS-CoV-2 S trimer. Our map unambiguously identifies that SNAP1 interacts exclusively with the NTD of SARS-CoV-2 S (Figure 2 B), in agreement with the results from BLI.

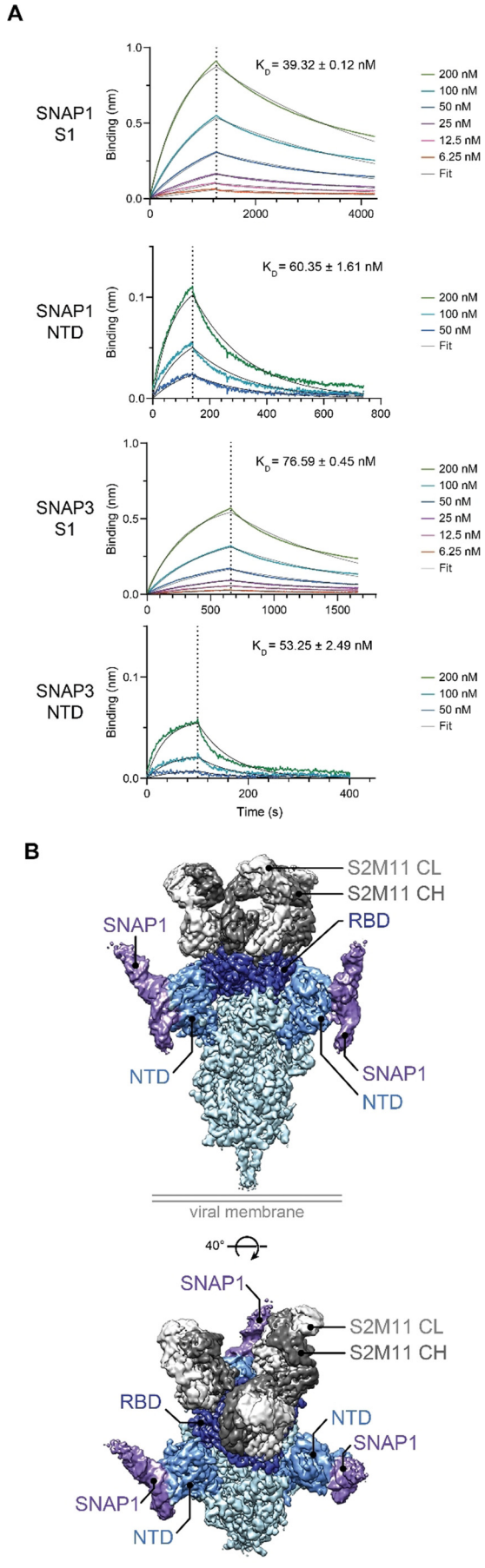

We obtained a 3.6 Å reconstruction for the region encompassing SNAP1 and part of SARS-CoV-2 S NTD (Figure S8D inset) through focused 3D classification and local refinement (Figure S8E). SNAP1 contacts residues 68–70, the NTD hairpin formed by residues 140–158, and a loop containing residues 253–257. These latter two regions are part of an antigenic supersite recognized by neutralizing NTD mAbs.[9a,16] Comparison of the structures of NTD in complex with S2L28, S2M28 or S2X333 Fabs (PDB: 7LXZ, 7LY2, 7LXY) and with SNAP1 shows that these regions on SARS-CoV-2 S NTD are highly dynamic and adopt different conformations upon binding to different molecules.[9a] We likely discovered two NTD-binding aptamers because the NTD antigenic supersite is exposed and differs the most compared to SARS-CoV and MERS-CoV S1. Our SELEX and immune systems of multiple individuals selected for binders to the NTD supersite, which highlights the importance of the NTD in immunity, vaccine design, and diagnostics applications.

Next, we investigated whether SNAP1 can bind to S protein variants. S-2P is a stabilized mutant that contains two proline mutations K986P and V987P[17] and recapitulates the native state of S on SARS-CoV-2[8a,18] (Figure S9A). We observed striking differences in binding kinetics between trimeric proteins S and S-2P (Figure S9B). SNAP1 bound to S with an on-rate 125-fold higher than that of S-2 (Table S5).

We also evaluated SNAP1 binding to the S protein from the B.1.1.7 virus variant (Table S6) which contains several deletions in the NTD that affect antibody neutralization (Figure S9B). The on-rate of S-B.1.1.7 association to SNAP1 immobilized on the biosensor was in between that of SARS-CoV-2 S and S-2P (S > S-B.1.1.7 > S-2P) (Table S5). However, we measured a very fast off-rate despite using a trimer, suggesting reduced affinity of SNAP1 to this variant.

Aptamer truncation has, in some cases, improved binding affinity while reducing synthesis cost.[19] Deleting 10 or 18 nucleotides (nt) of the constant region from each end of SNAP1 did not perturb predicted structures of the random region (Figure S10A). The truncated SNAP1.66 (20 nt deletion, 66 nt total length) and SNAP1.50 (50 nt total length) aptamers have similar equilibrium binding constants as untruncated SNAP1 to both SARS-CoV-2 S1 and NTD (Figure S10B, Table S5).

Finally, we applied SNAP1 in LFA and ELISA for aptamer-based detection of SARS-CoV-2 S protein and UV-inactivated SARS-CoV-2. Capitalizing on the trimeric nature of the S protein, we used SNAP1.50 as both the capture and

Figure 2. SNAP1 and SNAP3 aptamers bind to the NTD of SARS-CoV-2 S protein. A) Kinetic and binding equilibrium constants were measured by BLI. Biotinylated aptamer loaded on streptavidin biosensors was associated with SARS-CoV-2 S1 or NTD. Dotted lines indicate switch from analyte association to dissociation. K_D values (mean ± s.d., $n = 5–6$) were determined from a global fit of the kinetic data for a 1:1 binding model. B) Two views of the S/SNAP1/S2M11 complex cryo-EM unsharpened map. SNAP1: purple, NTD: light blue, RBD: dark blue, rest of SARS-CoV-2 S: cyan, S2M11 CH (Fab fragment heavy chain): dark gray, S2M11 CL (Fab fragment light chain): light gray.

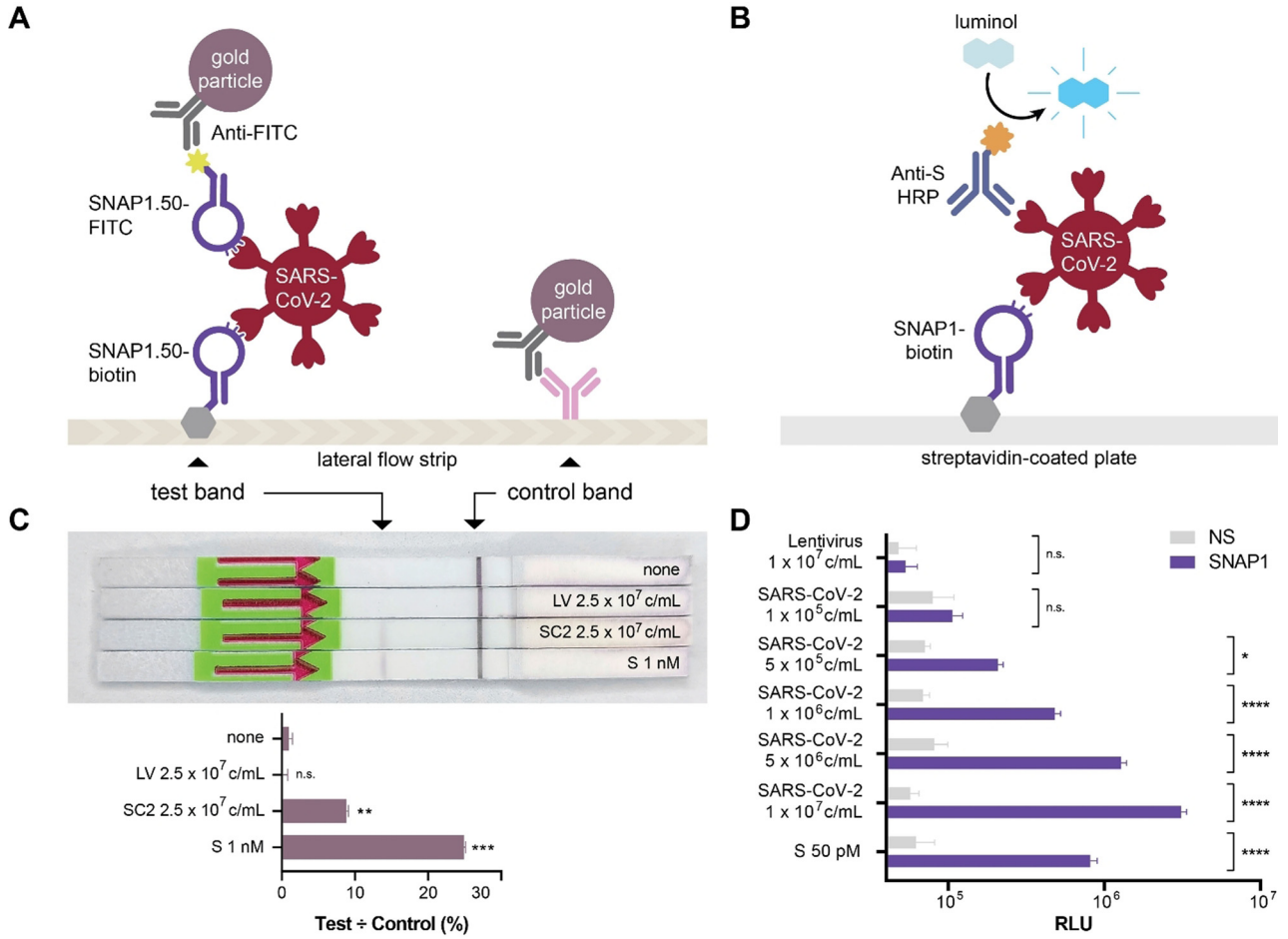

Figure 3. Aptamer-based detection of UV-inactivated SARS-CoV-2 virus. A) Schematic of HybriDetect LFA. B) Schematic of aptamer-antibody sandwich ELISA. C,D) c mL^{-1} = copies per mL of virus. C) HybriDetect LFA strips were dipped in solutions of S protein (S), control lentivirus (LV), or UV-inactivated SARS-CoV-2 virus (SC2) incubated with SNAP1.50. Top: representative image of developed strips. Bottom: quantification of band intensity. Bar graph shows mean and standard deviation of three replicates. Statistical comparison of LV, SC2, and S to none was determined by one-way ANOVA with Bonferroni correction, *** denotes $p < 0.001$, ** denotes $p < 0.01$, and n.s. denotes no significance. D) ELISA using NS-biotin or SNAP1-biotin as capture agents to detect UV-inactivated SARS-CoV-2 using anti-S HRP antibody for detection. Bar graph shows mean and standard deviation of three replicates. Statistical comparison of NS to SNAP1 was determined by two-way ANOVA with Fisher's LSD test, **** denotes $p < 0.0001$, * denotes $p < 0.05$, and n.s. denotes no significance.

detection agent in the HybriDetect LFA (Figure 3A). We also performed a modified ELISA using SNAP1 to capture SARS-CoV-2 S protein (Figure 3B). We were able to detect as low as 250 pM of SARS-CoV-2 S with LFA (Figure S11A) and 10 pM S protein with ELISA (Figure S11B). The LFA detected UV-inactivated SARS-CoV-2 virus but not lentivirus at 2.5×10^7 copies mL^{-1} (Figure 3C). The ELISA detected UV-inactivated SARS-CoV-2 at concentrations as low as 5×10^5 copies mL^{-1} (Figure 3D). The concentration of SARS-CoV-2 RNA detected in saliva and nasopharyngeal samples from COVID-19 positive patients by RT-qPCR in the first two weeks after onset of symptoms ranged from 10^4 to 10^{10} copies mL^{-1}.[20] Therefore, SNAP1 can potentially detect SARS-CoV-2 in patient samples in a clinically relevant scenario. Potential approaches for further improving sensitivity in future diagnostic designs using SNAP1 include multimerizing the aptamer, including an amplification step, or using alternative detection modalities.[6a,21]

In summary, we discovered novel SARS-CoV-2-binding aptamers, characterized binding through real-time kinetics measurements and high resolution cryo-EM, and detected SARS-CoV-2 by LFA and ELISA. Due to the relatively short time frame required for selection, aptamer SELEX can be a first response platform for creating diagnostic agents for emerging diseases.

Acknowledgements

This work was supported by a University of Washington Population Health Initiative grant and NIH 1U01AA029316, NIH (R01GM120553, DP1AI158186 and HHSN272201700059C to D.V.), a Pew Biomedical Scholars Award (D.V.), Investigators in the Pathogenesis of Infectious Disease Awards from the Burroughs Wellcome Fund (D.V.), Fast Grants (D.V.), the University of Washington Arnold and Mabel Beckman Center for Cryo-EM, and the Natural

Sciences and Engineering Research Council of Canada (M.M.) We thank NIH RADx-Radical Data Coordination Center (DCC) at University of California San Diego (funded under NIH grant # 1U24LM013755-01) for the SARS-Related Coronavirus 2, Isolate USA-WA1/2020, NR-52281 deposited by the Centers for Disease Control and Prevention and obtained through BEI Resources, NIAID. We thank Lauren Carter from the Institute of Protein Design (IPD) who kindly produced S-2P protein through support from the Bill and Melinda Gates Foundation.

Conflict of Interest

We have provisional patent filed on the aptamer sequences in this manuscript.

Keywords: aptamers · coronavirus · cryo-EM · immunoassays · SARS-CoV-2

[1] a) F. Wu, S. Zhao, B. Yu, Y.-M. Chen, W. Wang, Z.-G. Song, Y. Hu, Z.-W. Tao, J.-H. Tian, Y.-Y. Pei, *Nature* **2020**, *579*, 265 – 269; b) P. Zhou, X.-L. Yang, X.-G. Wang, B. Hu, L. Zhang, W. Zhang, H.-R. Si, Y. Zhu, B. Li, C.-L. Huang, *Nature* **2020**, *579*, 270 – 273; c) N. Zhu, D. Zhang, W. Wang, X. Li, B. Yang, J. Song, X. Zhao, B. Huang, W. Shi, R. Lu, *N. Engl. J. Med.* **2020**, *382*, 727.

[2] A. Spinelli, G. Pellino, *Br. J. Surg.* **2020**, *107*, 785 – 787.

[3] J. H. Kim, F. Marks, J. D. Clemens, *Nat. Med.* **2021**, *27*, 205 – 211.

[4] S. Simpson, M. C. Kaufmann, V. Glozman, A. Chakrabarti, *Lancet Infect. Dis.* **2020**, *20*, e108 – e115.

[5] J. Joung, A. Ladha, M. Saito, N.-G. Kim, A. E. Woolley, M. Segel, R. P. Barretto, A. Ranu, R. K. Macrae, G. Faure, *N. Engl. J. Med.* **2020**, *383*, 1492 – 1494.

[6] a) J. Dinnes, J. J. Deeks, S. Berhane, M. Taylor, A. Adriano, C. Davenport, S. Dittrich, D. Emperador, Y. Takwoingi, J. Cunningham, *Cochrane Database of Systematic Reviews* **2021**; b) S. Lambert-Niclot, A. Cuffel, S. Le Pape, C. Vauloup-Fellous, L. Morand-Joubert, A.-M. Roque-Afonso, J. Le Goff, C. Delaugerre, *J. Clin. Microbiol.* **2020**, *58*, e00977 – 00920.

[7] M. Pavelka, K. Van-Zandvoort, S. Abbott, K. Sherratt, M. Majdan, C. Covid, I. Z. Analýz, P. Jarčuška, M. Krajčí, S. Flasche, *Science* **2021**, *372*, 635 – 641.

[8] a) A. C. Walls, Y.-J. Park, M. A. Tortorici, A. Wall, A. T. McGuire, D. Veesler, *Cell* **2020**, *181*, 281 – 292, e286; b) Y.-Z. Zhang, E. C. Holmes, *Cell* **2020**, *181*, 223 – 227.

[9] a) M. McCallum, A. De Marco, F. A. Lempp, M. A. Tortorici, D. Pinto, A. C. Walls, M. Beltramello, A. Chen, Z. Liu, F. Zatta, *Cell* **2021**, *184*, 2332 – 2347, e2316; b) M. A. Tortorici, N. Czudnochowski, T. N. Starr, R. Marzi, A. C. Walls, F. Zatta, J. E. Bowen, S. Jaconi, Z. Wang, A. De Marco, *bioRxiv* **2021**; c) T. N. Starr, N. Czudnochowski, F. Zatta, Y.-J. Park, Z. Liu, A. Addetia, D. Pinto, M. Beltramello, P. Hernandez, A. J. Greaney, *bioRxiv* **2021**; d) L. Piccoli, Y.-J. Park, M. A. Tortorici, N. Czudnochowski, A. C. Walls, M. Beltramello, C. Silacci-Fregni, D. Pinto, L. E. Rosen, J. E. Bowen, *Cell* **2020**, *183*, 1024 – 1042, e1021; e) M. A. Tortorici, M. Beltramello, F. A. Lempp, D. Pinto, H. V. Dang, L. E. Rosen, M. McCallum, J. Bowen, A. Minola, S. Jaconi, *Science* **2020**, *370*, 950 – 957; f) D. Pinto, Y.-J. Park, M. Beltramello, A. C. Walls, M. A. Tortorici, S. Bianchi, S. Jaconi, K. Culap, F. Zatta, A. De Marco, *Nature* **2020**, *583*, 290 – 295.

[10] a) L. R. Baden, H. M. El Sahly, B. Essink, K. Kotloff, S. Frey, R. Novak, D. Diemert, S. A. Spector, N. Rouphael, C. B. Creech, *N. Engl. J. Med.* **2021**, *384*, 403 – 416; b) L. A. Jackson, E. J. Anderson, N. G. Rouphael, P. C. Roberts, M. Makhene, R. N. Coler, M. P. McCullough, J. D. Chappell, M. R. Denison, L. J. Stevens, *N. Engl. J. Med.* **2020**, *383*, 1920 – 1931.

[11] a) F. Li, *Annu. Rev. Virol.* **2016**, *3*, 237 – 261; b) M. A. Tortorici, D. Veesler, *Adv. Virus Res.* **2019**, *105*, 93 – 116.

[12] a) D. H. Bunka, P. G. Stockley, *Nat. Rev. Microbiol.* **2006**, *4*, 588 – 596; b) L. I. Hernandez, I. Machado, T. Schafer, F. J. Hernandez, *Curr. Top. Med. Chem.* **2015**, *15*, 1066 – 1081; c) J. Zhou, J. Rossi, *Nat. Rev. Drug Discovery* **2017**, *16*, 181 – 202.

[13] a) D. L. Robertson, G. F. Joyce, *Nature* **1990**, *344*, 467 – 468; b) A. D. Ellington, J. W. Szostak, *Nature* **1990**, *346*, 818 – 822; c) C. Tuerk, L. Gold, *Science* **1990**, *249*, 505 – 510; d) K. Sefah, D. Shangguan, X. Xiong, M. B. O'donoghue, W. Tan, *Nat. Protoc.* **2010**, *5*, 1169 – 1185; e) M. R. Gotrik, T. A. Feagin, A. T. Csordas, M. A. Nakamoto, H. T. Soh, *Acc. Chem. Res.* **2016**, *49*, 1903 – 1910; f) J. Liu, M. You, Y. Pu, H. Liu, M. Ye, W. Tan, *Curr. Med. Chem.* **2011**, *18*, 4117 – 4125.

[14] a) Y. Song, J. Song, X. Wei, M. Huang, M. Sun, L. Zhu, B. Lin, H. Shen, Z. Zhu, C. Yang, *Anal. Chem.* **2020**, *92*, 9895 – 9900; b) M. Sun, S. Liu, X. Wei, S. Wan, M. Huang, T. Song, Y. Lu, X. Weng, Z. Lin, H. Chen, *Angew. Chem. Int. Ed.* **2021**, *60*, 10266 – 10272; *Angew. Chem.* **2021**, *133*, 10354 – 10360.

[15] K. K. Alam, J. L. Chang, D. H. Burke, *Mol. Ther. Nucleic Acids* **2015**, *4*, e230.

[16] a) Y. Chi, J. Remsik, V. Kiseliovas, C. Derderian, U. Sener, M. Alghader, F. Saadeh, K. Nikishina, T. Bale, C. Iacobuzio-Donahue, *Science* **2020**, *369*, 276 – 282; b) L. Zhang, L. Cao, X. Gao, B. Zheng, Y. Deng, J.-X. Li, R. Feng, Q. Bian, X.-L. Guo, N. Wang, *bioRxiv* **2020**; c) W. N. Voss, Y. J. Hou, N. V. Johnson, G. Delidakis, J. E. Kim, K. Javanmardi, A. P. Horton, F. Bartzoka, C. J. Paresi, Y. Tanno, *Science* **2021**, *372*, 1108 – 1112.

[17] a) R. N. Kirchdoerfer, N. Wang, J. Pallesen, D. Wrapp, H. L. Turner, C. A. Cottrell, K. S. Corbett, B. S. Graham, J. S. McLellan, A. B. Ward, *Sci. Rep.* **2018**, *8*, 1 – 11; b) J. Pallesen, N. Wang, K. S. Corbett, D. Wrapp, R. N. Kirchdoerfer, H. L. Turner, C. A. Cottrell, M. M. Becker, L. Wang, W. Shi, *Proc. Natl. Acad. Sci. USA* **2017**, *114*, E7348 – E7357.

[18] Z. Ke, J. Oton, K. Qu, M. Cortese, V. Zila, L. McKeane, T. Nakane, J. Zivanov, C. J. Neufeldt, B. Cerikan, *Nature* **2020**, *588*, 498 – 502.

[19] a) N. Kacherovsky, I. I. Cardle, E. L. Cheng, L. Y. Jonathan, M. L. Baldwin, S. J. Salipante, M. C. Jensen, S. H. Pun, *Nat. Biomed. Eng.* **2019**, *3*, 783 – 795; b) A. Schmitz, A. Weber, M. Bayin, S. Breuers, V. Fieberg, M. Famulok, G. Mayer, *Angew. Chem. Int. Ed.* **2021**, *60*, 10279 – 10285; *Angew. Chem.* **2021**, *133*, 10367 – 10373.

[20] A. L. Wyllie, J. Fournier, A. Casanovas-Massana, M. Campbell, M. Tokuyama, P. Vijayakumar, J. L. Warren, B. Geng, M. C. Muenker, A. J. Moore, *N. Engl. J. Med.* **2020**, *383*, 1283 – 1286.

[21] a) H. Kuai, Z. Zhao, L. Mo, H. Liu, X. Hu, T. Fu, X. Zhang, W. Tan, *J. Am. Chem. Soc.* **2017**, *139*, 9128 – 9131; b) P. Dauphin-Ducharme, K. Yang, N. Arroyo-Currás, K. L. Ploense, Y. Zhang, J. Gerson, M. Kurnik, T. E. Kippin, M. N. Stojanovic, K. W. Plaxco, *ACS Sens.* **2019**, *4*, 2832 – 2837; c) N. K. Singh, P. Ray, A. F. Carlin, C. Magallanes, S. C. Morgan, L. C. Laurent, E. S. Aronoff-Spencer, D. A. Hall, *Biosens. Bioelectron.* **2021**, *180*, 113111; d) J. Deng, F. Tian, C. Liu, Y. Liu, S. Zhao, T. Fu, J. Sun, W. Tan, *J. Am. Chem. Soc.* **2021**, *143*, 7261 – 7266.

Manuscript received: June 9, 2021
Accepted manuscript online: July 30, 2021
Version of record online: August 18, 2021

